Rock Mechanics and Rock Engineering (2021) 54:921–935
https://doi.org/10.1007/s00603-020-02293-y

ORIGINAL PAPER

A Unified Constitutive Model for Rock Based on Newly Modified GZZ Criterion

Haohua Chen[1] · Hehua Zhu[2] · Lianyang Zhang[1]

Received: 4 May 2020 / Accepted: 26 October 2020 / Published online: 19 November 2020

Abstract

This paper proposes a unified constitutive model for rock based on the newly modified generalized Zhang-Zhu (GZZ) criterion. The constitutive model adopts a non-associated plastic flow rule and a continuous potential function that takes the three effective principal stresses into account. To reflect strain-softening, strain-hardening, and elastic-perfectly plastic behavior of rock in a unified way, a general expression is proposed to model the post-failure behavior of rock using the deviatoric plastic shear strain as the fundamental variable. The proposed constitutive model has been successfully implemented in a 3D finite-difference code and validated using it to simulate the true triaxial test of two types of rocks and comparing the simulation results with the experimental data. Finally, a 3D numerical model based on the proposed constitutive model is constructed to simulate a highway rock tunnel during construction. The results show that the predicted displacements of the rock tunnel are in good agreement with the field measurements.

Keywords Rock · 3D hoek–brown criterion · Constitutive model · Strain-softening · Strain-hardening

List of Symbols

E_{rm}	Young's modulus of rock mass
I_1^*, I_2^*, I_3^*	Transformed first, second and third stress invariants
J_2, J_3	Second and third deviatoric stress invariants
m_b, s, a	Material constant for rock masses defined in Hoek–Brown criterion
m_{bi}, m_{br}	Initial and residual value of m_b
m_d	Material constant defining potential function
m_{di}, m_{dr}	Initial and residual value of m_d
m_i	Material constant for the intact rock
p'	Mean effective stress
s_i, s_r	Initial and residual value of s
ε_f	A parameter controlling the softening/hardening of the yield function
ε_g	A parameter controlling the evolution of the potential function
ε_q^p	Plastic deviatoric shear strain
$\varepsilon_x, \varepsilon_y, \varepsilon_z, \varepsilon_{xy}, \varepsilon_{xz}, \varepsilon_{yz}$	Six basic strain components
θ_σ	Lode's angle
$\sigma_1', \sigma_2', \sigma_3'$	Maximum, intermediate, and minimum effective principal stresses
σ_c	Unconfined compressive strength of intact rock
$\sigma_{m,2}'$	Effective mean stress
$\sigma_x', \sigma_y', \sigma_z', \tau_{xy}, \tau_{xz}, \tau_{yz}$	Six basic stress components
τ_{oct}	Octahedral shear stress
D	Disturbance factor reflecting the level of blast damage and stress relaxation to rock mass
E, v	Young's modulus and Poisson's ratio
GSI	Geological strength index
K, G	Bulk modulus and shear modulus
f, g	Yield function and potential function
λ	Plastic multiplier for flow rule
ε	$[\varepsilon_x, \varepsilon_y, \varepsilon_z, 2\varepsilon_{xy}, 2\varepsilon_{xz}, 2\varepsilon_{yz}]$
σ	$\left[\sigma_x', \sigma_y', \sigma_z', \tau_{xy}, \tau_{xz}, \tau_{yz}\right]$

✉ Lianyang Zhang
lyzhang@email.arizona.edu

[1] Department of Civil and Architectural Engineering and Engineering Mechanics, The University of Arizona, Tucson, AZ 85716, USA

[2] Department of Geotechnical Engineering, Tongji University, Shanghai 200092, China

1 Introduction

Modeling rock behavior is one of the most important problems in rock mechanics and rock engineering (Zhang 2016). Much work has been carried out during the past decades regarding the constitutive model for rock. Singh (1973) proposed a constitutive model for jointed rock mass based on the assumption that discontinuities can be seen as staggered joints and the intact rock between the joints deforms elastically. Following the same idea, other empirical equations or flow rule functions on the joints were proposed to model the jointed rock mass (Gens et al. 1990; Cai and Horii 1992; Sitharam et al. 2001; Zandarin et al. 2013). However, those constitutive models apply to the joints rather than the whole rock mass, and the assumed elastic behavior for the intact rock between joints can result in the overestimation of rock stability.

To take the rock mass as a whole, it is of great importance to consider the strength of rock mass under a true triaxial stress condition rather than the failure stress in only one specific direction. The Hoek–Brown strength criterion (Hoek and Brown 1980, 1988; Hoek et al. 2002) is one of the most popular empirical failure criteria in rock mechanics due to its accuracy and wide applicability to different types of rock masses. However, the effective intermediate principal stress, σ_2', is ignored in the Hoek–Brown criterion, which may cause inaccurate predictions under true triaxial stress states in practical applications. To overcome this limitation, many researchers have proposed 3D versions of the Hoek–Brown criterion by considering the effect of σ_2' (Pan and Hudson 1988; Priest 2005, 2012; Zhang and Zhu 2007; Jiang et al. 2011; Zhang et al. 2013; Wu et al. 2018). Among those 3D criteria, the generalized Zhang-Zhu (GZZ) criterion (Zhang and Zhu 2007; Zhang 2008) can reduce to the 2D Hoek–Brown criterion and has a simple and explicit form. To solve the non-smoothness and non-convexity problems of the GZZ criterion, Zhang et al. (2013) successfully extended the GZZ criterion to a version with a smooth and convex surface. However, the modified GZZ criterion is not in a simple, explicit form and a numerical iterative procedure is required for determining the aspect ratio, a parameter used by Zhang et al. (2013) to define the shape of the criterion in π-plane. To tackle the non-smoothness and non-convexity problems more simply, a newly modified GZZ criterion with an explicit formulation expressed by the three stress invariants was proposed by Chen et al. (2019). In this paper, the newly modified GZZ criterion is adopted as the yield function for developing the unified constitutive model for rock.

The current commercial finite element (FE) and finite difference (FD) codes mainly use constitutive models based on the 2D Hoek–Brown criterion for rock. Although the strain hardening/softening behavior of soil, metal, and concrete can be properly considered, these codes usually only provide simple elastic-perfectly plastic constitutive models for rock masses (Itasca 2017; Brinkgreve et al. 2013; ABAQUS 2015; LSTC 2017). Therefore, this paper proposes a unified constitutive model based on the newly modified GZZ criterion, which considers not only the 3D strength but also the strain-softening, strain-hardening and elastic-perfectly plastic behavior of rock in a general way. The proposed constitutive model has been implemented in an FD code, FLAC3D, and validated by applying it to simulate the true triaxial test of two types of rocks and comparing the simulation results with the experimental data. Finally, the constitutive model is utilized to analyze a highway rock tunnel during construction to check its applicability to practical engineering problems.

2 Newly Modified GZZ Criterion

To provide the background information for developing the new constitutive model, this section briefly describes and discusses the Hoek–Brown criterion and the newly modified GZZ criterion.

The original Hoek–Brown criterion is given as (Hoek and Brown 1980):

$$\sigma_1' = \sigma_3' + \sigma_c\left(m_i\frac{\sigma_3'}{\sigma_c} + 1\right)^{0.5}, \tag{1}$$

where σ_1' and σ_3' are the maximum and minimum effective principal stresses, respectively; σ_c denotes the unconfined compressive strength (UCS) of the intact rock; and m_i is a material constant for the intact rock.

For jointed rock masses, the generalized Hoek–Brown criterion, which takes both the fracture and rock mass conditions into account, is expressed as (Hoek et al. 1992):

$$\sigma_1' = \sigma_3' + \sigma_c\left(m_b\frac{\sigma_3'}{\sigma_c} + s\right)^{a}, \tag{2}$$

where m_b denotes a material constant for rock masses; and a and s are two constants reflecting the characteristics of the rock masses. The three parameters can be determined by the empirical relations (Hoek et al. 2002):

$$m_b = m_i \cdot \exp\left(\frac{\mathrm{GSI}-100}{28-14D}\right), \tag{3a}$$

$$s = \exp\left(\frac{\mathrm{GSI}-100}{9-3D}\right), \tag{3b}$$

$$a = \frac{1}{2} + \frac{1}{6}\left[\exp\left(-\frac{\mathrm{GSI}}{15}\right) - \exp\left(-\frac{20}{3}\right)\right], \tag{3c}$$

where GSI is the geological strength index (GSI) (Hoek et al. 2002); and D is the disturbance factor representing the level of blast damage and stress relaxation to the rock mass.

Considering that the intermediate principal stress can have a significant effect on the strength of rock (Mogi 1971; Pan and Hudson 1988), Zhang and Zhu (2007) proposed a 3D version of the Hoek–Brown criterion with $a = 0.5$. Later on, Zhang (2008) extended it to a generalized form for all a values:

$$\frac{1}{\sigma_c^{(1/a-1)}}\left(\frac{3}{\sqrt{2}}\tau_{\mathrm{oct}}\right)^{1/a} + \frac{m_b}{2}\left(\frac{3}{\sqrt{2}}\tau_{\mathrm{oct}}\right) - m_b\sigma'_{m,2} = s\sigma_c, \tag{4}$$

where τ_{oct} is the octahedral shear stress and $\sigma'_{m,2}$ denotes the effective mean stress, which are determined by:

$$\tau_{\mathrm{oct}} = \frac{1}{3}\sqrt{\left(\sigma'_1 - \sigma'_2\right)^2 + \left(\sigma'_2 - \sigma'_3\right)^2 + \left(\sigma'_3 - \sigma'_1\right)^2}, \tag{5a}$$

$$\sigma'_{m,2} = \frac{\sigma'_1 + \sigma'_3}{2}, \tag{5b}$$

where σ'_2 is the intermediate effective principal stress. The generalized 3D criterion (Eq. 4) has been named the generalized Zhang-Zhu criterion (Priest 2012) and, to be simple, is called the GZZ criterion in this paper.

The GZZ criterion uses the same parameters as the Hoek–Brown criterion and can reduce to the Hoek–Brown criterion under both triaxial compression (TC) and triaxial extension (TE) conditions, but it is neither smooth at the TC or TE state nor convex at the TE state. Therefore, Zhang et al. (2013) adopted three smooth and convex Lode dependences to replace the original Lode dependence of the GZZ criterion to address the non-smoothness and non-convexity problems. The modified GZZ criterion is given as:

$$\sqrt{J_2} = L\left(\theta_\sigma\right)_{X-D}\sqrt{J_{2,\max}};\ \ X = E, H \text{ and } S, \tag{6}$$

where J_2 is the second deviatoric stress invariant defined by:

$$J_2 = \frac{1}{6}\left[\left(\sigma'_1 - \sigma'_2\right)^2 + \left(\sigma'_2 - \sigma'_3\right)^2 + \left(\sigma'_3 - \sigma'_1\right)^2\right] = \frac{3}{2}\tau_{\mathrm{oct}}^2. \tag{7a}$$

The subscripts E, H and S stand for the dependencies using elliptical approximation, hyperbolic expression and spatial mobilized plane, respectively, which are expressed by:

$$L\left(\theta_\sigma\right)_{E-D} = \frac{2(1-\delta^2)\cos(\frac{\pi}{6}-\theta_\sigma)+(2\delta-1)\sqrt{4(1-\delta^2)\cos^2(\frac{\pi}{6}-\theta_\sigma)+\delta(5\delta-4)}}{4(1-\delta^2)\cos^2(\frac{\pi}{6}-\theta_\sigma)+(2\delta-1)^2}, \tag{7b}$$

$$L\left(\theta_\sigma\right)_{H-D} = \frac{2\delta(1-\delta^2)\cos(\frac{\pi}{6}+\theta_\sigma)+\delta(\delta-2)\sqrt{4(\delta^2-1)\cos^2(\frac{\pi}{6}+\theta_\sigma)+(5-4\delta)}}{4(1-\delta^2)\cos^2(\frac{\pi}{6}+\theta_\sigma)-(\delta-2)^2}, \tag{7c}$$

$$L\left(\theta_\sigma\right)_{S-D} = \frac{\sqrt{3}\delta}{2\sqrt{\delta^2-\delta+1}}\frac{1}{\cos\psi};\psi = \begin{cases} \frac{1}{6}\arccos\left[-1 + \frac{27\delta^2(1-\delta)^2}{2(\delta^2-\delta+1)^3}\sin^2(3\theta_\sigma)\right], \text{ for } \theta_\sigma \geq 0 \\ \frac{\pi}{3} - \frac{1}{6}\arccos\left[-1 + \frac{27\delta^2(1-\delta)^2}{2(\delta^2-\delta+1)^3}\sin^2(3\theta_\sigma)\right], \text{ for } \theta_\sigma < 0 \end{cases}, \tag{7d}$$

$$\delta = \sqrt{\frac{J_{2,\min}}{J_{2,\max}}} = \sqrt{\frac{J_2\left(-\frac{\pi}{6}\right)}{J_2\left(\frac{\pi}{6}\right)}}, \tag{7e}$$

$$\theta_\sigma = \frac{1}{3}\sin^{-1}\left(\frac{3\sqrt{3}J_3}{2J_2^{3/2}}\right), \tag{7f}$$

$$J_3 = \left(\sigma'_1 - p'\right)\left(\sigma'_2 - p'\right)\left(\sigma'_3 - p'\right), \tag{7g}$$

$$p' = \frac{\sigma'_1 + \sigma'_2 + \sigma'_3}{3}, \tag{7h}$$

For a given rock, $J_{2,\max}$ and $J_{2,\min}$, in the same π plane, can be determined from an explicit expression if $a = 0.5$, but an iterative algorithm is needed when $a \neq 0.5$. This can result in difficulty in implementing the criterion in FE or FD codes.

To address the non-smoothness and non-convexity problems in a simpler way and with an explicit function, Chen et al. (2019) further modified the GZZ criterion as below:

$$\frac{1}{\sigma_c^{(1/a-1)}}\left(\frac{3}{\sqrt{2}}\tau_{\mathrm{oct}}\right)^{1/a} + \frac{m_b}{2}\left(\frac{3}{\sqrt{2}}\tau_{\mathrm{oct}}\right) - \frac{m_b}{2}\sqrt{\frac{18I_1^{*3}\tau_{\mathrm{oct}}^2 - 81I_1^*\tau_{\mathrm{oct}}^4 - 54I_3^*\tau_{\mathrm{oct}}^2}{4I_1^{*3} - 18I_1^*\tau_{\mathrm{oct}}^2 - 108I_3^*}} = 0, \tag{8}$$

where

$$I_1^* = 3p^* = \sigma_1^* + \sigma_2^* + \sigma_3^* = I_1 + 3\frac{\sigma_c}{m_b}s, \tag{9a}$$

$$I_3^* = \sigma_1^*\sigma_2^*\sigma_3^* = \left(\sigma'_1 + \frac{\sigma_c}{m_b}s\right)\left(\sigma'_2 + \frac{\sigma_c}{m_b}s\right)\left(\sigma'_3 + \frac{\sigma_c}{m_b}s\right). \tag{9b}$$

The newly modified GZZ criterion (Chen et al. 2019) can be seen as a 3D version of the Hoek–Brown criterion using the same parameters. Furthermore, the explicit expression with a smooth and convex shape in the π-plane makes it easier to be implemented into FE and FD codes than both the Hoek–Brown criterion (Hoek et al. 2002) and the modified GZZ criterion (Zhu et al. 2017). Therefore, the newly modified GZZ criterion by Chen et al. (2019) is adopted as the yield function for the proposed constitutive model.

3 Constitutive Model Based on the Newly Modified GZZ Criterion

3.1 Fundamentals of Plasticity and Return Mapping

In the theory of plasticity, the total strain increment can be decomposed into an elastic part and a plastic part (Owen and Hinton 1980):

$$d\varepsilon = d\varepsilon^e + d\varepsilon^p, \tag{10a}$$

$$\varepsilon = \left[\varepsilon_x, \varepsilon_y, \varepsilon_z, 2\varepsilon_{xy}, 2\varepsilon_{xz}, 2\varepsilon_{yz}\right], \tag{10b}$$

where $d\varepsilon$ is the total strain increment; $d\varepsilon^e$ is the elastic strain increment, and $d\varepsilon^p$ is the plastic strain increment. $d\varepsilon^p$ does not occur when the stress state is within the yield surface f, while both $d\varepsilon^e$ and $d\varepsilon^p$ happen after yielding.

According to Hooke's law, the stress increment caused by the elastic strain increment can be defined as:

$$d\sigma = Dd\varepsilon^e = D(d\varepsilon - d\varepsilon^p), \tag{11a}$$

$$\sigma = \left[\sigma'_x, \sigma'_y, \sigma'_z, \tau_{xy}, \tau_{xz}, \tau_{yz}\right], \tag{11b}$$

where D is the elastic constitutive matrix with respect to Young's modulus E and Poisson's ratio v as follows:

$$D = \begin{bmatrix} a_1 & a_2 & a_2 & & & \\ a_2 & a_1 & a_2 & & & \\ a_2 & a_2 & a_1 & & & \\ & & & G & & \\ & & & & G & \\ & & & & & G \end{bmatrix}, \tag{12a}$$

$$a_1 = K + \tfrac{4}{3}G, \tag{12b}$$

$$a_2 = K - \tfrac{2}{3}G, \tag{12c}$$

$$K = \tfrac{E}{3(1-2v)}, \tag{12d}$$

$$G = \tfrac{E}{2(1+v)}. \tag{12e}$$

Equation (11a) can also be written as:

$$d\sigma = Dd\varepsilon^e = D(d\varepsilon - d\varepsilon^p) = d\sigma^e - d\sigma^p, \tag{13}$$

which indicates that the stress increment can also be decomposed to an elastic part, $d\sigma^e$, and a plastic part, $d\sigma^p$.

As shown in Fig. 1, when the stress state (point A) is within but close to the yield curve ($f=0$), a small strain increment may result in the initial trial stress state (point B) falling outside the yield surface (i.e., $f(\sigma_B) > 0$). For the estimation of the initial trial stress state, it is assumed that no plastic strain occurs and thus σ_B can be calculated using incremental elasticity as:

$$\sigma_B = \sigma_A + Dd\varepsilon. \tag{14}$$

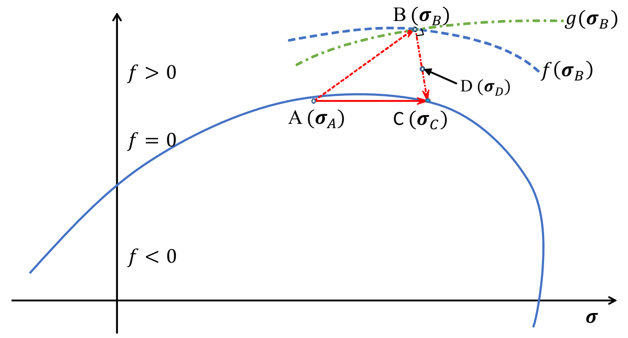

Fig. 1 Schematic diagram of return mapping method. (After Clausen and Damkilde 2008)

Then a so-called plastic corrector stress increment, $\Delta\sigma^p$, is needed to drag the stress state (point B) back to the yield surface (point C), which can be described as:

$$\sigma_C = \sigma_B - \Delta\sigma^p = \sigma_B - Dd\varepsilon^p = \sigma_A + D(d\varepsilon - d\varepsilon^p). \tag{15}$$

Equations (14) and (15) are the so-called return mapping method (Clausen and Damkilde 2008). According to the flow rule, the plastic strain increment can be expressed as:

$$d\varepsilon^p = d\lambda \tfrac{\partial g}{\partial \sigma}, \tag{16}$$

where $d\lambda$ denotes the plastic multiplier and g is the potential function. When $g = f$, the flow rule is associated and if $g \neq f$, it is non-associated.

Hence, the aforementioned plastic corrector stress increment can be formulated as

$$\Delta\sigma^p = \int_\lambda^{\lambda+\Delta\lambda} D \tfrac{\partial g}{\partial \sigma} d\lambda = \Delta\lambda D \left.\tfrac{\partial g}{\partial \sigma}\right|_D, \tag{17}$$

where $\Delta\lambda$ is the incremental form of $d\lambda$ and $\left.\frac{\partial g}{\partial \sigma}\right|_D$ means the value of $\frac{\partial g}{\partial \sigma}$ at point D which should be between points B and C. For convenience and simplification consideration, point D can be taken as point B or C if the strain increment is infinitesimal. It should be noted that the derivation of g at B or C yields the same value for a liner potential function, but substituting $\left.\frac{\partial g}{\partial \sigma}\right|_B$ for $\left.\frac{\partial g}{\partial \sigma}\right|_D$ in a non-linear potential function, such as the Hoek–Brown criterion, can cause a radical return (Krieg and Krieg 1977).

Since point C is located on the yield surface f,

$$f\left(\sigma_C\right) = 0. \tag{18}$$

By solving Eq. (18), the value of the plastic multiplier can be determined; then by substituting $\Delta\lambda$ back into Eqs. (15) and (17), the final stress state at point C can be determined.

3.2 Constitutive Model Based on Newly Modified GZZ Criterion

Following the classical plasticity theory, the isotropic elastic behavior of the proposed constitutive model obeys Hooke's law expressed by Eqs. (12a–e) and (13). Since the yield function, Eq. (8), contains a square root term, a negative value of the expression inside can lead to non-convergence of the constitutive model during return mapping. To solve the possible non-convergence problem and increase the speed of convergence, Eq. (8) is rewritten as:

$$f = \left[\left(\frac{q}{\sigma_c}\right)^{2/a-2} + m_b\left(\frac{q}{\sigma_c}\right)^{1/a-1}\right]\left(I_1^* I_2^* - 9I_3^*\right) - 2m_b^2 I_3^* = 0, \tag{19}$$

where

$$q = \sqrt{I_1^{*2} - 3I_2^*}, \tag{20a}$$

$$I_2^* = \sigma_1^*\sigma_2^* + \sigma_2^*\sigma_3^* + \sigma_3^*\sigma_1^*. \tag{20b}$$

Similarly, the potential function of the proposed constitutive model is defined as follows:

$$g = \left[\left(\frac{q}{\sigma_c}\right)^{2/a-2} + m_d\left(\frac{q}{\sigma_c}\right)^{1/a-1}\right]\left(I_1^* I_2^* - 9I_3^*\right) - 2m_d^2 I_3^* = 0, \tag{21}$$

where m_d is a material constant of rock. When m_d is equal to m_b, the flow rule is associated; otherwise, the flow rule is non-associated.

To implement the return mapping algorithm, an expression for the plastic multiplier $\Delta\lambda$ needs to be derived. As shown in Eq. (11b), there are six basic stress components involved in the updating of the stress state, which makes it complicated for derivation. FLAC3D determines the effective principal stresses through the getEigenInfo() function by solving the following equations:

$$\sigma_1' + \sigma_2' + \sigma_3' = I_1 = \sigma_x' + \sigma_y' + \sigma_z', \tag{22a}$$

$$\sigma_1'\sigma_2' + \sigma_2'\sigma_3' + \sigma_3'\sigma_1' = I_2 = \sigma_x'\sigma_y' + \sigma_y'\sigma_z' + \sigma_z'\sigma_x' - \tau_{xy}^2 - \tau_{yz}^2 - \tau_{xz}^2, \tag{22b}$$

$$\sigma_1'\sigma_2'\sigma_3' = I_3 = \sigma_x'\sigma_y'\sigma_z' + 2\tau_{xy}\tau_{xz}\tau_{yz} - \tau_{xy}^2\sigma_z' - \tau_{yz}^2\sigma_x' - \tau_{xz}^2\sigma_y'. \tag{22c}$$

The stress state of point B will first be expressed as a principal stress tensor and then returned to point C via the return mapping algorithm. Finally, the principal stresses of point C will be converted back to the corresponding six stress components using the resolve() function. Therefore, the derivations below will use only the three principal stresses.

According to the flow rule and Eq. (15),

$$d\sigma_1^{*p} = d\sigma_1^p = d\lambda\left[a_1\frac{\partial g}{\partial\sigma_1} + a_2\frac{\partial g}{\partial\sigma_2} + a_2\frac{\partial g}{\partial\sigma_3}\right], \tag{23a}$$

$$d\sigma_2^{*p} = d\sigma_2^p = d\lambda\left[a_2\frac{\partial g}{\partial\sigma_1} + a_1\frac{\partial g}{\partial\sigma_2} + a_2\frac{\partial g}{\partial\sigma_3}\right], \tag{23b}$$

$$d\sigma_3^{*p} = d\sigma_3^p = d\lambda\left[a_2\frac{\partial g}{\partial\sigma_1} + a_2\frac{\partial g}{\partial\sigma_2} + a_1\frac{\partial g}{\partial\sigma_3}\right], \tag{23c}$$

where

$$\frac{\partial g}{\partial\sigma_i} = \frac{3}{2}\frac{\partial g}{\partial q}\frac{\sigma_i - p}{q} + \frac{\partial g}{\partial I_1^*} + \frac{\partial g}{\partial I_2^*}\left(I_1^* - \sigma_i^*\right) + \frac{\partial g}{\partial I_3^*}\frac{I_3^*}{\sigma_i^*}; i = 1,2,3, \tag{24a}$$

$$\frac{\partial g}{\partial q} = \frac{1}{q}\left[2\frac{1-a}{a}\left(\frac{q}{\sigma_c}\right)^{2/a-2} + m_b\frac{1-a}{a}\left(\frac{q}{\sigma_c}\right)^{1/a-1}\right]\left(I_1^* I_2^* - 9I_3^*\right), \tag{24b}$$

$$\frac{\partial g}{\partial I_1^*} = \left[\left(\frac{q}{\sigma_c}\right)^{2/a-2} + m_d\left(\frac{q}{\sigma_c}\right)^{1/a-1}\right] I_2^*, \tag{24c}$$

$$\frac{\partial g}{\partial I_2^*} = \left[\left(\frac{q}{\sigma_c}\right)^{2/a-2} + m_d\left(\frac{q}{\sigma_c}\right)^{1/a-1}\right] I_1^*, \tag{24d}$$

$$\frac{\partial g}{\partial I_3^*} = -9\left[\left(\frac{q}{\sigma_c}\right)^{2/a-2} + m_d\left(\frac{q}{\sigma_c}\right)^{1/a-1}\right] - 2m_d^2. \tag{24e}$$

Substitution of Eqs. (23a–c) into Eq. (17) yields,

$$\sigma_{1C}^* = \sigma_{1B}^* - \Delta\sigma_1' = \sigma_{1B}^* - \Delta\lambda\left[a_1\left.\frac{\partial g}{\partial\sigma_1'}\right|_D + a_2\left.\frac{\partial g}{\partial\sigma_2'}\right|_D + a_2\left.\frac{\partial g}{\partial\sigma_3'}\right|_D\right], \tag{25a}$$

$$\sigma_{2C}^* = \sigma_{2B}^* - \Delta\sigma_2' = \sigma_{2B}^* - \Delta\lambda\left[a_2\left.\frac{\partial g}{\partial\sigma_1'}\right|_D + a_1\left.\frac{\partial g}{\partial\sigma_2'}\right|_D + a_2\left.\frac{\partial g}{\partial\sigma_3'}\right|_D\right], \tag{25b}$$

$$\sigma_{3C}^* = \sigma_{3B}^* - \Delta\sigma_3' = \sigma_{3B}^* - \Delta\lambda\left[a_2\left.\frac{\partial g}{\partial\sigma_1'}\right|_D + a_2\left.\frac{\partial g}{\partial\sigma_2'}\right|_D + a_1\left.\frac{\partial g}{\partial\sigma_3'}\right|_D\right]. \tag{25c}$$

Since point C should be located on the yield surface, Eqs. (25a–c) can be placed in Eq. (19) and the resulted equation can then be solved to determine the multiplier, $\Delta\lambda$. For an infinitesimal stress increment,

$$f(\sigma_C) - f(\sigma_B) = \Delta f = -\left.\frac{\partial f}{\partial\sigma_1'}\right|_B \Delta\sigma_1' - \left.\frac{\partial f}{\partial\sigma_2'}\right|_B \Delta\sigma_2' - \left.\frac{\partial f}{\partial\sigma_3'}\right|_B \Delta\sigma_3'. \tag{26}$$

Substitution of Eqs. (25a–c) into Eq. (26) yields,

$$\Delta\lambda = \frac{f(\sigma_B)}{a_2\left(\left.\frac{\partial g}{\partial\sigma_1'}\right|_D + \left.\frac{\partial g}{\partial\sigma_2'}\right|_D + \left.\frac{\partial g}{\partial\sigma_3'}\right|_D\right)\left(\left.\frac{\partial f}{\partial\sigma_1'}\right|_B + \left.\frac{\partial f}{\partial\sigma_2'}\right|_B + \left.\frac{\partial f}{\partial\sigma_3'}\right|_B\right) + G\left(\left.\frac{\partial f}{\partial\sigma_1'}\right|_B \left.\frac{\partial g}{\partial\sigma_1'}\right|_D + \left.\frac{\partial f}{\partial\sigma_2'}\right|_B \left.\frac{\partial g}{\partial\sigma_2'}\right|_D + \left.\frac{\partial f}{\partial\sigma_3'}\right|_B \left.\frac{\partial g}{\partial\sigma_3'}\right|_D\right)}. \tag{27}$$

Since Eq. (27) is derived under the condition of an infinitesimal stress increment, too large an error may be induced if the stress increment is not small enough. Therefore, the following iterative algorithm is proposed for determining $\Delta\lambda$:

(1) Calculate an initial value of plastic multiplier $\Delta\lambda$, denoted as $(\Delta\lambda)_1$, from Eq. (27) and set $j = 1$;
(2) Calculate the updated stress state at point C:

$$\sigma_C = \sigma_B - (\Delta\lambda)_j D \left.\frac{\partial g}{\partial \sigma}\right|_B;\ j = 1,2,3,\ldots \tag{28}$$

(3) Calculate the new plastic multiplier $\Delta\lambda$ using Newton's method, denoted as $(\Delta\lambda)_{j+1}$:

$$(\Delta\lambda)_{j+1} = (\Delta\lambda)_j - \frac{f\left[(\Delta\lambda)_j\right]}{f'\left[(\Delta\lambda)_j\right]};\ j = 1,2,3,\ldots \tag{29}$$

where

$$f\left[(\Delta\lambda)_j\right] = \left[\left(\frac{(q_C)_j}{\sigma_c}\right)^{2/a-2} + m_b\left(\frac{(q_C)_j}{\sigma_c}\right)^{1/a-1}\right]\left(\left(I_{1C}^*\right)_j\left(I_{2C}^*\right)_j - 9\left(I_{3C}^*\right)_j\right) - 2m_b^2\left(I_{3C}^*\right)_j, \tag{30a}$$

$$f'\left[(\Delta\lambda)_j\right] = G\left.\frac{\partial f}{\partial\sigma_i'}\right|_C\left.\frac{\partial g}{\partial\sigma_i'}\right|_B + a_2\left(\left.\frac{\partial f}{\partial\sigma_1'}\right|_C + \left.\frac{\partial f}{\partial\sigma_2'}\right|_C + \left.\frac{\partial f}{\partial\sigma_3'}\right|_C\right)\left(\left.\frac{\partial g}{\partial\sigma_1'}\right|_B + \left.\frac{\partial g}{\partial\sigma_2'}\right|_B + \left.\frac{\partial g}{\partial\sigma_3'}\right|_B\right), \tag{30b}$$

and update j: $j = j + 1$;
(4) Check the yield function f as follows:

$$\left|\frac{f\left[(\Delta\lambda)_j\right]}{\sigma_c^3}\right| \le \epsilon, \tag{31}$$

where ϵ is a prescribed convergence limit, i.e., 0.0001. If Eq. (31) is not satisfied, steps (2)–(4) are repeated. After Eq. (31) is satisfied, $\Delta\lambda = (\Delta\lambda)_j$ and the stress state is then calculated with Eq. (28).

3.3 General Strain-Softening and Strain-Hardening Rule

The post-failure of rock can be classified into three types: strain-softening, perfectly plastic and strain-hardening as shown in Fig. 2, with the corresponding parameters defined below and listed in Table 1. To characterize the three types of post-failures in a unified way, the deviatoric shear plastic strain ε_q^p is selected as the fundamental variable and a general exponential function as shown in Fig. 3a is used to describe the evolution of the parameters in the yield function f. In the figure, x can be m_b, s or m_d. For example, for m_b and s, we have

$$m_b = m_{\mathrm{br}} + \left(m_{\mathrm{bi}} - m_{\mathrm{br}}\right)e^{-3\frac{\varepsilon_q^p}{\varepsilon_f}}, \tag{32a}$$

$$s = s_r + \left(s_i - s_r\right)e^{-3\frac{\varepsilon_q^p}{\varepsilon_f}}, \tag{32b}$$

where the subscript i and r denote the initial value and residual value of rock parameters m_b and s; ε_f is the plastic deviatoric strain at which the yield function would almost evolve to the corresponding residual state f; and ε_q^p is the plastic deviatoric shear strain defined by:

$$\varepsilon_q^p = \int d\varepsilon_q^p, \tag{33a}$$

$$d\varepsilon_q^p = \sqrt{\frac{\left(d\varepsilon_1^p - d\varepsilon_2^p\right)^2 + \left(d\varepsilon_2^p - d\varepsilon_3^p\right)^2 + \left(d\varepsilon_3^p - d\varepsilon_1^p\right)^2}{2}}, \tag{33b}$$

The potential function, g, shares the same parameters a and s as the yield function, f. In this case, if $m_d = m_b$, the

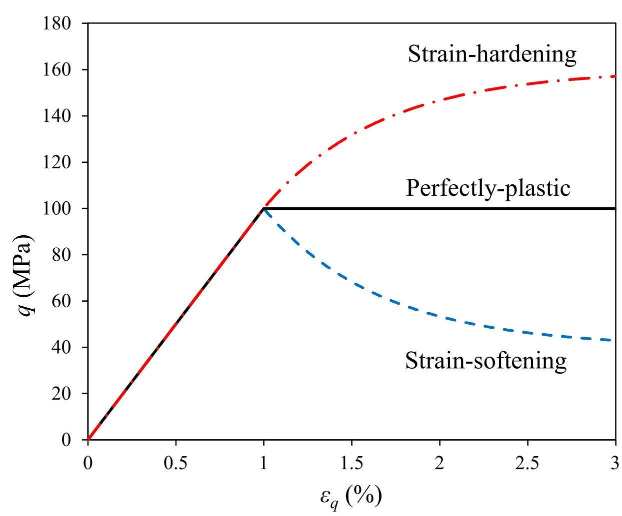

Fig. 2 Three types of post-failures of rock (the related parameters are listed in Table 1)

Table 1 Material parameters for strain-hardening, elastic-perfectly-plastic and strain softening models shown in Fig. 1

Type	σ_c (MPa)	a	E (GPa)	v	m_{bi}	m_{br}	s_{bi}	s_{br}	m_{di}	m_{dr}	ε_f (%)	ε_g (%)
EPP	50	0.5	13	0.3	10	10	1	1	10	10	–	–
SH	50	0.5	13	0.3	10	30.8	1	1	10	30.8	2	2
SS	50	0.5	13	0.3	10	1.13	1	0.3	10	1.13	2	2

$\sigma_2' = \sigma_3' = 15$ MPa

EPP elastic-perfectly plastic, *SH* strain hardening, *SS* strain softening

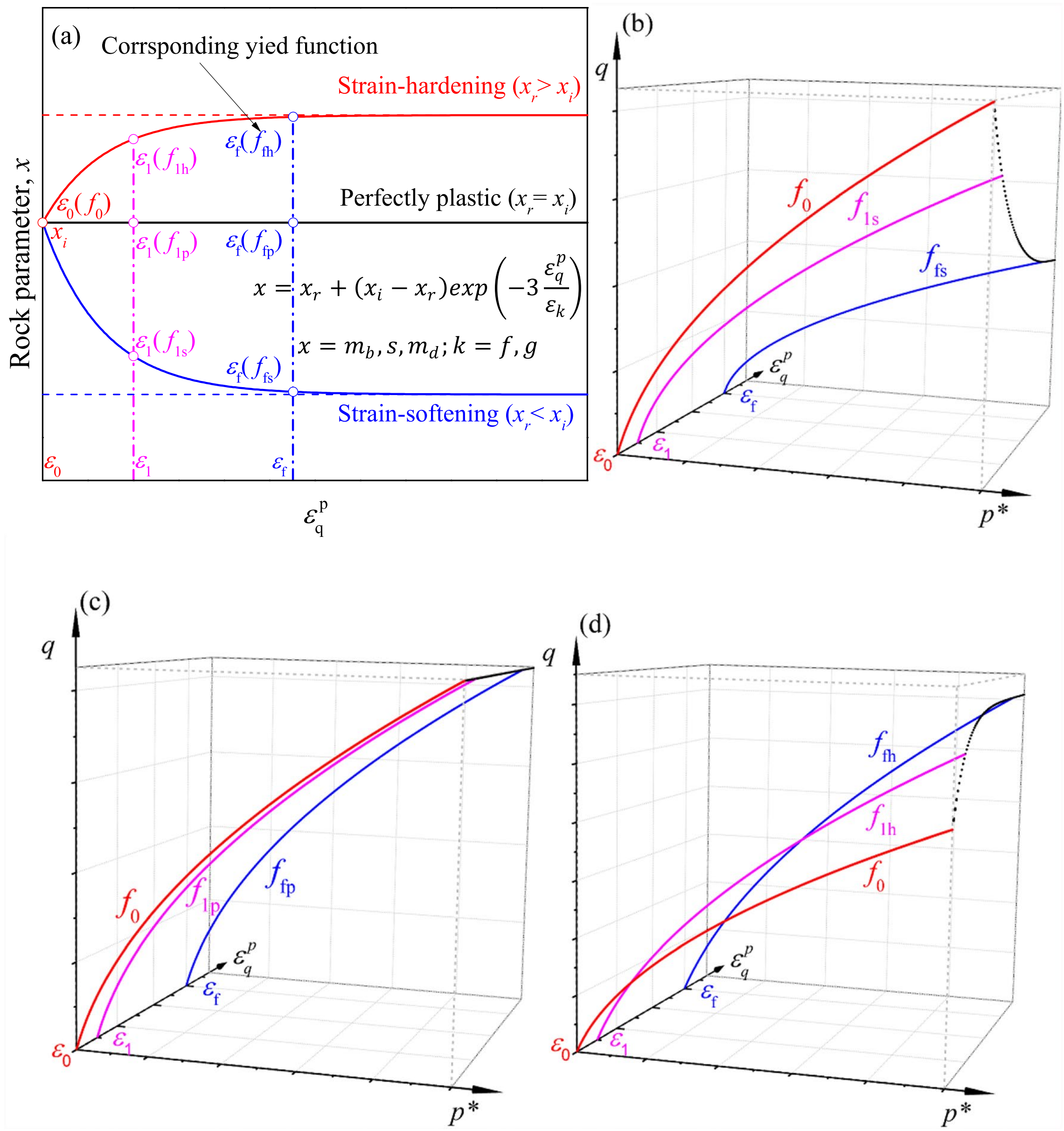

Fig. 3 **a** Relation between rock parameter and plastic deviatoric shear strain; and Evolution of yield function in p^*–q–ε_q^p space for: **b** strain-softening; **c** perfectly-plastic; and **d** strain-hardening

constitutive model is associated. Otherwise, the constitutive model is non-associated. Similar to m_b, the evolution of m_d is defined by:

$$m_d = m_{\mathrm{dr}} + \left(m_{\mathrm{di}} - m_{\mathrm{dr}}\right)e^{-3\frac{\varepsilon_q^p}{\varepsilon_g}} \tag{34}$$

where ε_g is the plastic deviatoric strain at which the potential function would almost evolve to its residual state.

Taking advantage of the general strain softening/hardening rule, the yield curve of the proposed constitutive model evolves with the increase of the plastic deviatoric shear strain in the p^*–q–ε_q^p space as shown in Fig. 3. When the stress state is within the yield surface, no plastic strain occurs and the yield function f_0, the red curve in Fig. 3b–d, is defined by the initial values of the rock material parameters. When the accumulated plastic deviatoric shear strain, ε_q^p, reaches a value, say ε_1 in Fig. 3a, the rock material parameters change as shown in Fig. 3a and the yield surface evolves to $f_{1\mathrm{s}}$, $f_{1\mathrm{p}}$ or $f_{1\mathrm{h}}$, the magenta curve in Fig. 3b–d depending on the type of post-failure. Finally, as ε_q^p almost approaches ε_f, the yield surface (blue curves in Fig. 3b–d in p^*–q–ε_q^p space would tend to the corresponding residual one.

In summary, the proposed unified constitutive model contains the following parameters:

- Young's modulus E and Poisson's ratio ν.
- Unconfined compressive strength σ_c.
- Parameters for the initial yield function: m_{bi}, s_i, a.
- Parameter for the initial potential function: m_{di}, s_i, a.
- Parameters for the residual yield function: m_{br}, s_r, a.
- Parameters for the residual potential function: m_{dr}, s_r, a.
- Parameters for controlling the rate of softening/hardening: ε_f, ε_g.

The determination of these parameters is discussed in the next section.

3.4 Determination of Model Parameters

For the application of the proposed constitutive model, the 12 parameters involved in it should be determined. The following describes the recommended procedure for determining the parameters of the proposed model for intact rock and rock mass, respectively.

3.4.1 Intact Rock

For intact rock, uniaxial (at least one) and triaxial (at least three) compression tests can be conducted for determining the parameters as follows:

(1) E, ν and σ_c can be determined from the test results by following the standard procedure (Hudson and Harrison 1997).
(2) m_{bi}, s_i, a are determined by fitting the peak strength data of the uniaxial and triaxial compression tests with the Hoek–Brown criterion with $s_i = 1$ and $a = 0.5$.
(3) m_{br} and s_r are determined by fitting the residual strength data of the uniaxial and triaxial compression tests with the Hoek–Brown criterion with $a = 0.5$.
(4) m_{di} and m_{dr} are determined based on the ratio of axial strain rate to lateral strain rate when the plastic strain takes place and when the stresses approach the final state from the triaxial compression tests, respectively.
(5) ε_f is the plastic deviatoric shear strain at which m_b and s approach m_{br} and s_r. Similarly, ε_g is the plastic deviatoric shear strain at which m_d approaches m_{dr}. Both can be determined from the stress–strain relation of the triaxial compression tests.

3.4.2 Rock Mass

In terms of rock mass, it is difficult and even impossible to perform the required large-scale tests for determining the various parameters. In this case, the empirical methods based on the GSI system and typical data ranges can be used.

(1) E, ν, σ_c, m_{bi}, and s_i, a can be determined using the method based on GSI from Hoek and Brown (2018). The deformation modulus of can be estimated by (Hoek and Diederichs 2006):

$$E_{\mathrm{rm}} = 10^5 \frac{1 - D/2}{1 + \exp[(75 + 25D - \mathrm{GSI})/11]} \quad (\mathrm{MPa}), \tag{35a}$$

or

$$E_{\mathrm{rm}} = E_i \left\{ 0.02 + \frac{1 - D/2}{1 + \exp[(60 + 15D - \mathrm{GSI})/11]} \right\} \quad (\mathrm{MPa}), \tag{35b}$$

in which, the initial GSI of the rock mass is determined by field observations and the disturbed factor D is estimated based on blast damage and stress relaxation; and E_i is the Young's modulus of the intact rock. The Poisson's ratio ν can be determined following Gercek (2007) and Zhang (2016). The unconfined compressive strength σ_c of the intact rock can be obtained from the uniaxial compression test in the lab. And m_{bi}, s_i, and a can be determined from Eqs. (3a–c) with known GSI and D.

(2) The residual strength parameters of the rock mass, m_{br} and s_r, can also be determined from Eqs. (3a–c), but the residual GSI, GSI_r, of the rock mass should be used. The GSI_r can be estimated following Cai et al. (2007). For example, the following simple equation from Cai et al. (2007) can be used:

$$\mathrm{GSI}_r = \mathrm{GSI} \times \exp(-0.0134\mathrm{GSI}), \tag{36}$$

in which, GSI is the initial GSI.

(3) As for m_{di} and m_{dr}, a value within the range of 0.4–1.0 m_{bi} can be selected for m_{di}, and a typical estimation of m_{dr} can be $m_{dr} = m_{br}$.
(4) A typical value of ε_f and ε_g should be in the range of 1–10% (Farmer 1983; Walton et al. 2014, 2017; Zhao and Cai 2010).

Some of the above recommendations for determining the model parameters, such as the range of ε_f and ε_g, are based on limited data. As more data are available, the range can be narrowed for specific rocks and the accuracy can be improved.

4 Validation of Proposed Constitutive Model

To validate the proposed constitutive model, it is implemented in finite-difference code FLAC3D and applied to simulate the true triaxial test of two types of rocks: Mizuho trachyte and Beishan granite.

4.1 Mizuho Trachyte

The true triaxial test results of Mizuho trachyte (Mogi 1971), the $\left(\sigma_1' - \sigma_3'\right)$ versus ε_1 and ε_3 versus ε_1 curves under different stress states are shown in Figs. 4 and 5, respectively. Based on the experimental $\left(\sigma_1' - \sigma_3'\right)$ versus ε_1 relation, the rock can be considered to follow the elastic-perfectly plastic constitutive model. In this case, the parameters of the constitutive model for simulating the true triaxial test of Mizuho trachyte are determined and summarized in Table 2.

The $\left(\sigma_1' - \sigma_3'\right)$ versus ε_1 relations from the simulation under different intermediate stresses are also shown in Fig. 4. The good agreement of the simulation results with the experimental data indicates that the elastic-perfectly plastic constitutive model can capture the stress–strain relation of Mizuho trachyte well. For further comparison, Fig. 5 shows the ε_3 versus ε_1 relations at different intermediate effective stresses from both experiments and simulations. The ε_3 versus ε_1 relations from the simulation are also in quite good agreement with those from the experiments.

4.2 Beishan Granite

For rock, strain-softening is a very common post-failure mode under true triaxial stress states. In this regard, the true triaxial test results of Beishan granite which shows strain-softening (Zhang et al. 2019) are selected for verification of the proposed constitutive model. Table 3 summarizes the rock parameters for the Beishan granite used for the numerical simulation.

Figure 6 shows the stress–strain curves from the true triaxial tests (Zhang et al. 2019) and those from the numerical simulations at different values of σ_3'. As can be seen, the Beishan granite exhibits strong brittle-ductile characteristics. ε_2 changes much less than ε_1 and ε_3 after the peak shear stress (during fracturing) because the failure (fracture) surfaces are parallel to the direction of σ_2' (Zhang et al. 2019). It can also be seen that the simulation results are in good agreement with those from the experiments. The predictions from elastic-perfectly plastic models such as Zhu et al. (2017) are not included for comparison

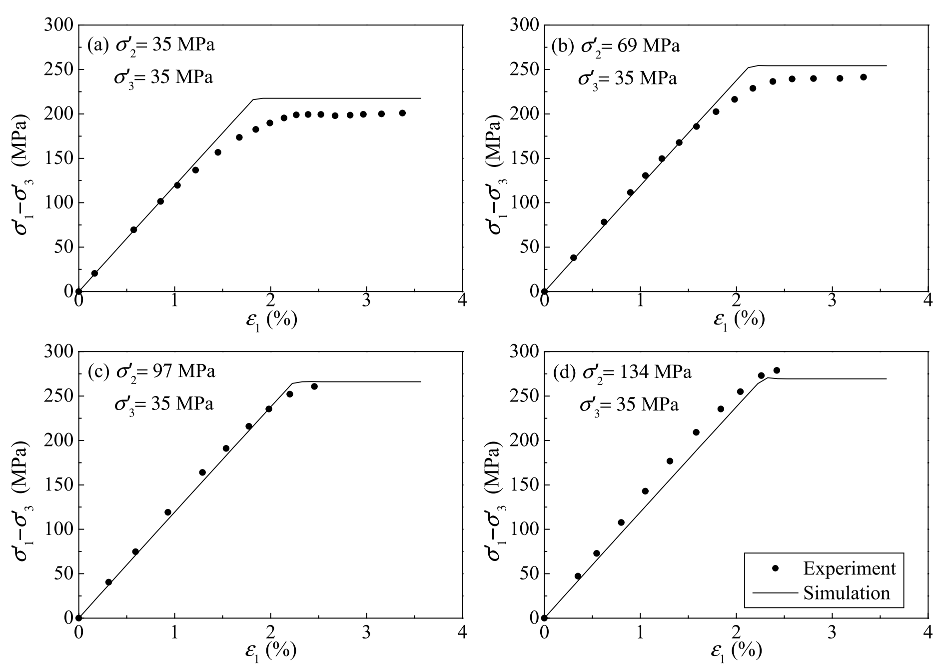

Fig. 4 Comparison of $\left(\sigma_1' - \sigma_3'\right)$ versus ε_1 of Mizuho trachyte from simulations and experiments

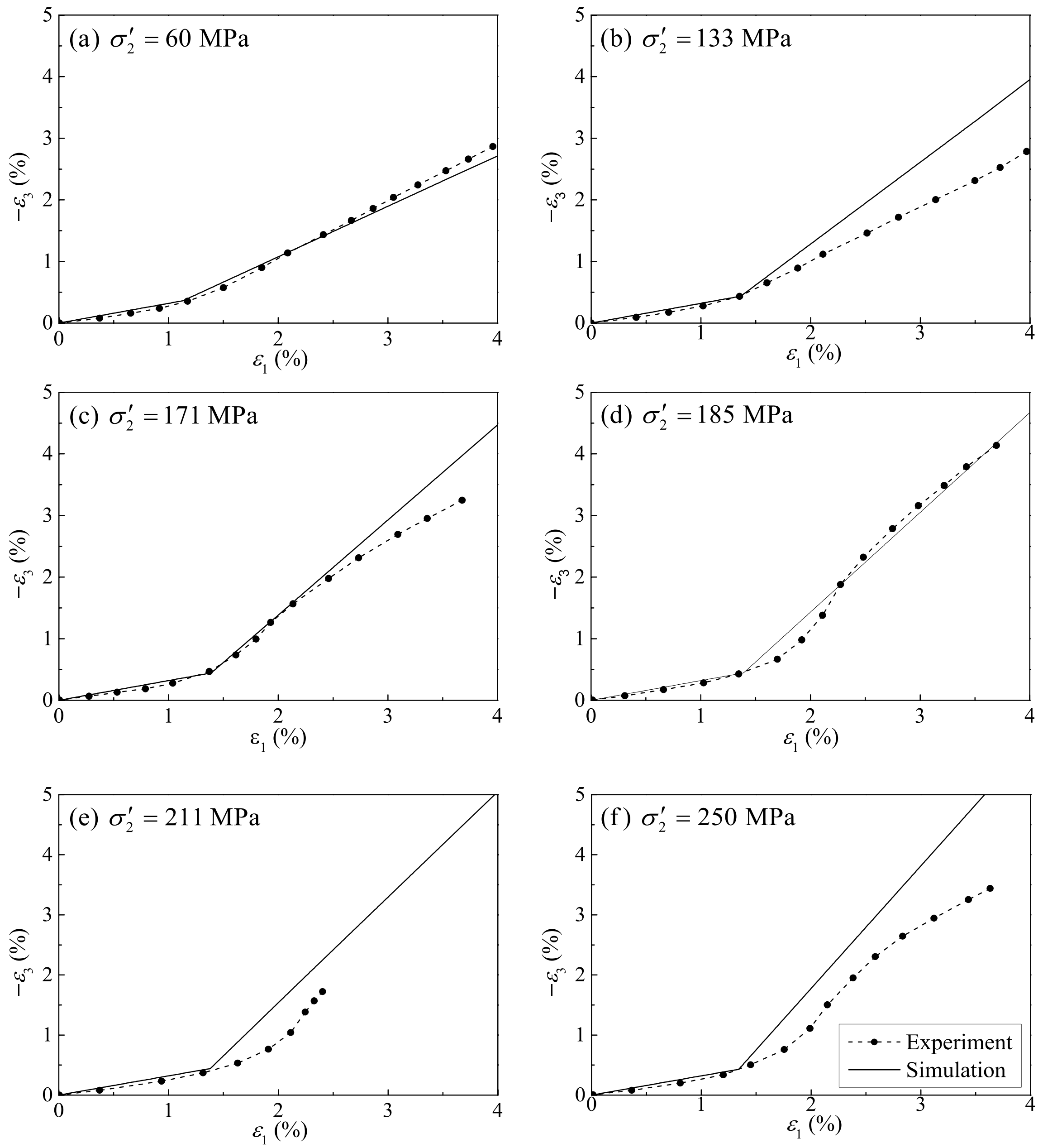

Fig. 5 Comparison of ε_1 versus ε_3 of Mizuho trachyte from simulations and experiments

Table 2 Material parameters for Mizuho trachyte

σ_c (MPa)	a	E (GPa)	ν	m_{bi}	m_{br}	s_{bi}	s_{br}	m_{di}	m_{dr}	ε_f (%)	ε_g (%)
100	0.5	25	0.27	10.55	10.55	1	1	3.485	3.485	–	–

Table 3 Material parameters for Beishan granite

σ_c (MPa)	a	E (GPa)	ν	m_{bi}	m_{br}	s_{bi}	s_{br}	m_{di}	m_{dr}	ε_f (%)	ε_g (%)
141	0.5	54	0.27	32.02	3.03	1	0.17	16	3	3	3

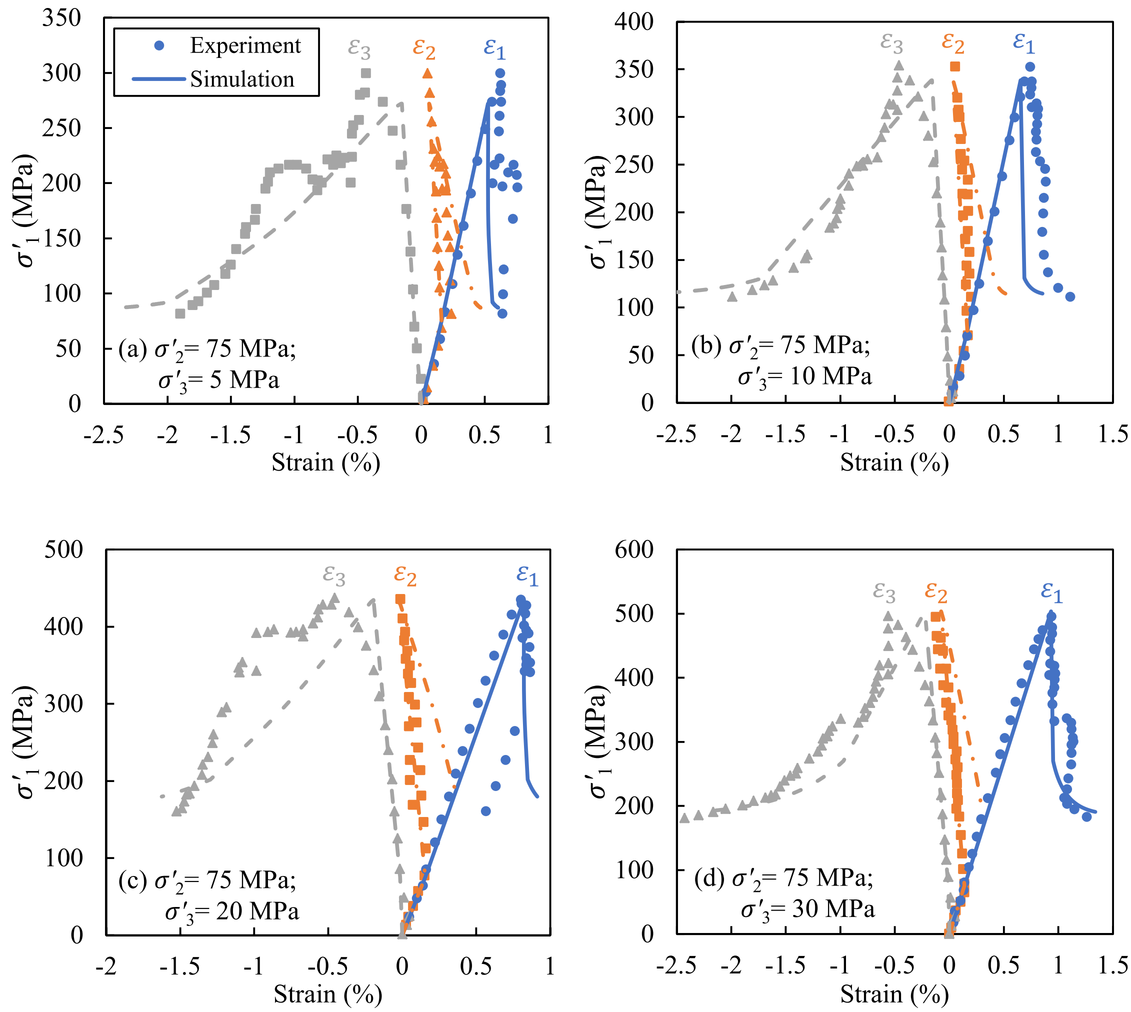

Fig. 6 Comparison of effective major principal stress versus strains of Beishan granite from simulations and experiments

because the predicted σ_1' would not change after failure and apparently cannot represent the strain-softening behavior of the rock. This is one of the major advantages of the proposed constitutive model over other perfectly plastic models.

5 Application of Proposed Constitutive Model

To further verify the applicability of the proposed constitutive model in practical engineering, it is used to analyze a highway rock tunnel during construction in Guizhou province, China. The tunnel is 8 km long and was constructed by the so-called top-heading-and-bench method. Two linings, one layer of plain concrete and one layer of reinforced concrete, were used to support the tunnel. To simplify the analysis, only a 50 m long section of the tunnel at a buried depth of around 140 m is considered. Considering the symmetry and to eliminate the effect of boundaries, a numerical model of 75 m × 140 m × 75 m as shown in Fig. 7 is constructed. The bottom boundary and the four side boundaries are constrained in the normal direction, and an equivalent normal uniform loading of 1.54 MPa based on rock mass unit weight and buried depth is applied at the top boundary to simulate the overburden. The in situ horizontal stress is assumed to be equal to the in situ vertical stress in the analysis. 110 steps of construction processes, including the up and down bench cut, the first lining installation, the second lining installation and backfilling, are considered in the analysis. The length of each bench and the first lining is 2 m, while one section of the second lining and backfill is 10 m long. The material properties of the two linings and the backfill are summarized in Table 4.

The in-situ rock is sandstone and the unconfined compressive strength, σ_c, of the intact rock is 13.2 MPa. According to Zhu et al. (2017), the material parameter m_i can be estimated as 17. Using the modified geological strength index (GSI)

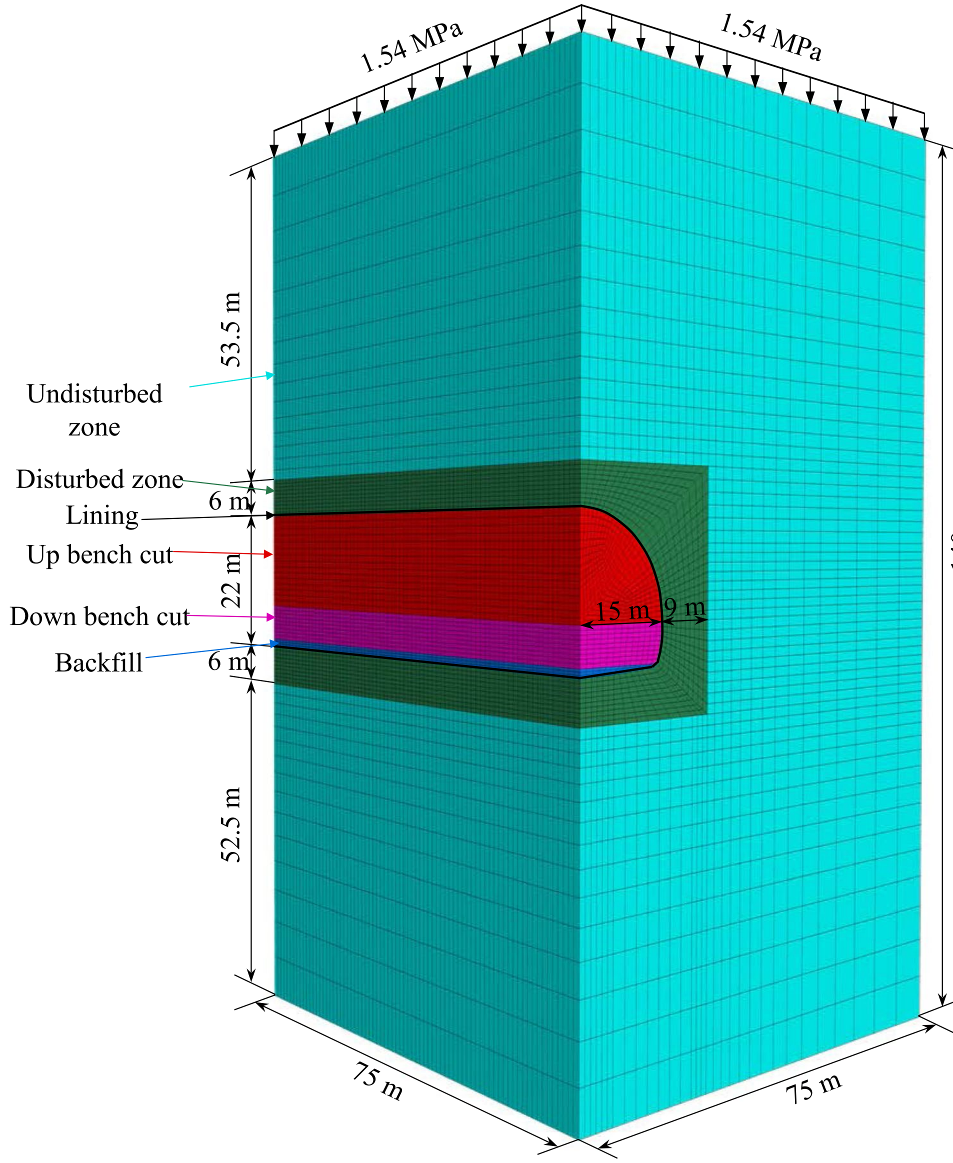

Fig. 7 Numerical model of tunnel

Table 4 Material parameters for initial lining, second lining, and backfill

Layer	Material type	Density (kg/m^3)	E (GPa)	ν	Thickness (m)
Initial lining	Plain concrete	2.2×10^3	21	0.25	0.2
Second lining	Reinforced concrete	2.5×10^3	29.5	0.25	0.4
Backfill	Plain concrete	2.4×10^3	26	0.25	1.2

Table 5 Material parameters for rock mass around the tunnel

Zone	Density (kg/m^3)	E (GPa)	ν	σ_c (MPa)	m_b	a	s	m_d
Disturbed	2.35×10^3	3.24	0.3	13.2	1.834	0.507	0.0014	1.834
Undisturbed	2.35×10^3	7.27	0.3	13.2	2.56	0.507	0.0027	2.56

For strain-softening model, $m_{\mathrm{br}} = m_{\mathrm{di}} = 0.73$, $s_r = 0.0001$, $\varepsilon_f = \varepsilon_g = 5\%$

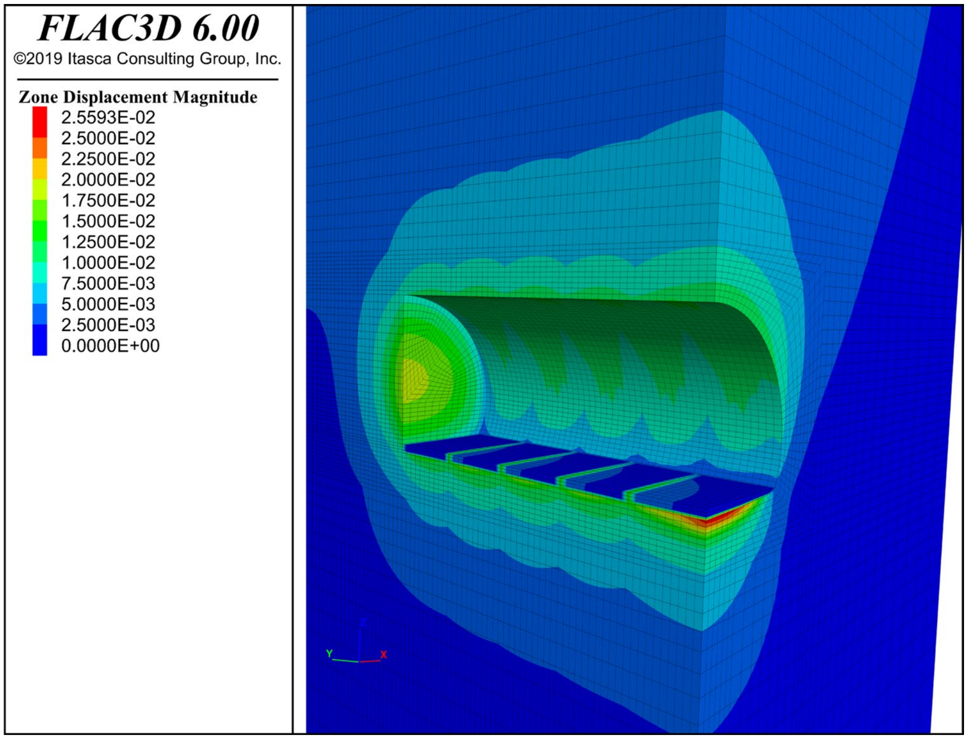

Fig. 8 Displacement contour of rock around tunnel after excavation

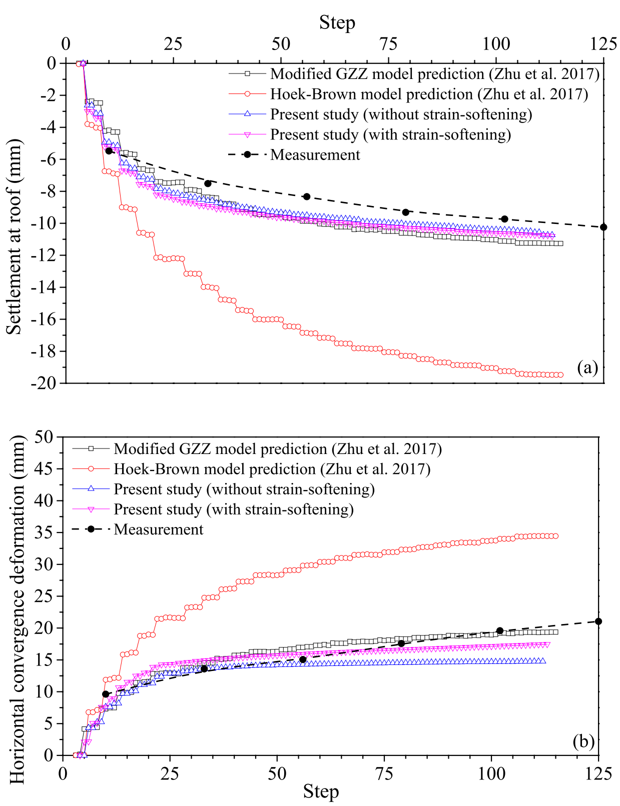

Fig. 9 Comparison of **a** tunnel roof displacement and **b** tunnel horizontal convergence deformation from field measurements and simulations

system (Sonmez and Ulusay 1999) and following Zhu et al. (2017), the GSI of the rock mass is 47. The tunnel was excavated by the blast drilling method, which could cause some disturbance to the surrounding rock. Therefore, a disturbance factor D of 0.3 is assumed for the disturbed zone. According to Hoek (2012), the disturbed zone of a 10 m diameter tunnel could extend as much as 3 m into the rock. Since the simulated tunnel is 30 m and 22 m in the horizontal and vertical directions, the disturbed zone is assumed to extend 9 m and 6 m from the tunnel into the rock along the horizontal and vertical directions, respectively (Fig. 7). Beyond the disturbed zone, the disturbance factor is assigned as 0. With the obtained m_i, GSI and D, the other parameters of the proposed constitutive model can be determined by Eqs. (3a–c). To be simple, m_d is selected to be equal to m_b. Since no information is available about the residual strength or strain-softening properties of the rock, the elastic-perfectly plastic model is used. The Young's modulus, E_{rm}, of both the disturbed and undisturbed zones are determined by (Hoek and Diederichs 2006). All the parameters for the rock mass are summarized in Table 5.

Figure 8 shows the displacement contour after excavation. For the roof and floor zones, the excavation would affect the rock mass within about one diameter from the tunnel, while in the horizontal direction, the excavation has much less influence on the surrounding rock mass. The maximum displacement occurs in the first section of the cut because this part was excavated first and affected by the whole excavation process.

Figure 9 shows the roof settlement and horizontal convergence deformation from the numerical analysis. For comparison, the field measurements and the numerical results based on the original Hoek–Brown constitutive model and the modified GZZ constitutive model from Zhu et al. (2017) are also shown in the figure. As can be seen, the roof settlement and the horizontal convergence deformation from the analysis based on the original Hoek–Brown constitutive model are both significantly larger than those from the field measurements. The roof settlement and the horizontal convergence deformation from the analyses based on the modified GZZ constitutive model and the proposed constitutive model, however, are in good agreement with those from the field measurements. The slight difference between the results from the analysis based on the modified GZZ constitutive model and those based on the proposed constitutive model could be due to the difference in the total number of elements used in the analyses, the different potential functions adopted, and the absence of undisturbed zone in the simulation of Zhu et al. (2017).

To explore the influence of strain-softening, a numerical simulation is performed using the strain-softening model within the disturbed zone. The residual GSI of the rock mass within the disturbed zone is estimated from Eq. (36) as 25 and $m_{\rm br}$ and s_r can be further determined from Eqs. (3a–c) as 0.728 and 0.0001. As for the rest parameters, $m_{\rm di} = m_{\rm bi}$, $m_{\rm dr} = m_{\rm br}$ and $\varepsilon_f = \varepsilon_g = 5\,\%$ following the recommendations in Sect. 3.3. The simulation results are also shown in Fig. 9. It can be seen that the accuracy of the predictions is slightly improved when the strain-softening is considered.

6 Conclusions

The major conclusions can be summarized below:

1. The unified constitutive model adopts a continuous potential function that takes the three effective principal stresses into account and a non-associated plastic flow rule. The three types of post-failure modes, strain-softening, strain-hardening and elastic-perfectly plastic, are described in a unified way using a general exponential expression.
2. The proposed constitutive model is implemented in a finite-difference code FLAC3D and used to simulate the true triaxial test of two types of rocks. The results indicate that the proposed constitutive model can effectively capture the stress–strain behavior of the rock in different directions.
3. The proposed constitutive model is successfully used to analyze a highway rock tunnel during construction. The predicted tunnel roof displacement and horizontal convergence deformation are in good agreement with the field measurements, indicating the applicability of the proposed constitutive model to practical engineering problems.

References

ABAQUS Inc. (2015) Abaqus analysis user's guide. Dassault Systems Simulia Corp, USA

Brinkgreve RBJ, Engine E, Swolfs WM (2013) Plaxis 3D user manual. Plaxis bv, NL

Cai M, Horii H (1992) A constitutive model of highly jointed rock masses. Mech Mater 13:217–246

Cai M, Kaiser PK, Tasaka Y, Minami M (2007) Determination of residual strength parameters of jointed rock masses using the GSI system. Int J Rock Mech Min Sci 44:247–265

Chen H, Zhu H, Zhang L (2019) Further modification of a generalized three-dimensional Hoek-Brown criterion. Manuscript submitted for publication

Clausen J, Damkilde L (2008) An exact implementation of the Hoek-Brown criterion for elasto-plastic finite element calculations. Int J Rock Mech Min Sci 45(6):831–847

Farmer IW (1983) Engineering behaviour of rocks. Chapman & Hall, London

Gens A, Carol I, Alonso E (1990) A constitutive model for rock joints formulation and numerical implementation. Comput Geotech 9(1):3–20

Gercek H (2007) Poisson's ratio values for rocks. Int J Rock Mech Min Sci 44:1–13

Hoek E (2012) Blast damage factor D. Technical note for RocNews, winter 2012 issue, RocScience, 2 Feb 2012

Hoek E, Brown ET (1980) Empirical strength criterion for rock masses. J Geotech Eng ASCE 106:1013–1035

Hoek E, Brown ET (1988) The Hoek–Brown criterion—a 1988 update. In: Proc. 15th Can. rock mech. symp., University of Toronto, Canada, pp 31–38

Hoek E, Brown ET (2018) The Hoek-Brown failure criterion and GSI—2018 edition. J Rock Mech Geotech Eng 11:445–463

Hoek E, Diederichs MS (2006) Empirical estimation of rock mass modulus. Int J Rock Mech Min Sci 43(2):203–215

Hoek E, Wood D, Shan S (1992) A modified Hoek–Brown criterion for jointed rock masses. In: Proceedings of the international ISRM symposium on rock characterization, Chester, UK, pp 209–214

Hoek E, Carranza-Torres C, Corkum B (2002) Hoek–Brown failure criterion—2002 edition. In: Hammah R et al (eds) Proc. 5th North American rock mech. symp. and 17th tunneling assoc. of Canada conf.: NARMS-TAC 2002. Min Innov Tech, Toronto, pp 267–273

Hudson JA, Harrison JP (1997) Rock engineering mechanics—an introduction to the principles. Elsevier, Oxford

Itasca Consulting Group Inc. (2017) Constitutive models. FLAC3D version 6.0, user's manual

Jiang H, Wang XW, Xie YL (2011) New strength criteria for rocks under polyaxial compression. Can Geotech J 48:1233–1245

Krieg RD, Krieg DB (1977) Accuracies of numerical solution methods for the elastic-perfectly plastic model. ASME J Press Vessel Technol 99:510–515

LSTC (Livermore Software Technology Corporation) (2017) LS-DYNA keyword user's manual volume I—III. Livermore, CA

Mogi K (1971) Fracture and flow of rocks under high triaxial compression. J Geophys Res 76(5):1255–1269

Owen DJR, Hinton E (1980) Finite elements in plasticity: theory and practice. Pineridge Press Limited, Swansea

Pan XD, Hudson JA (1988) A simplified three dimensional Hoek-Brown yield criterion. In: Romana M (ed) Rock mechanics and power plants. Balkema, Rotterdam, pp 95–103

Priest SD (2005) Determination of shear strength and three-dimensional yield strength for the Hoek-Brown yield criterion. Rock Mech Rock Eng 38(4):299–327

Priest SD (2012) Three-dimensional failure criteria based on the Hoek-Brown criterion. Rock Mech Rock Eng 45:989–993

Singh B (1973) Continuum characterization of jointed rock masses. Part 1—the constitutive equations. Int J Rock Mech Min Sci Geomech Abstr 22(4):197–213

Sitharam TG, Shimizu N, Sridevi J (2001) Practical equivalent continuum characterization of jointed rock masses. Int J Rock Mech Min Sci 38(3):437–448

Sonmez H, Ulusay R (1999) Modification to the geological strength index (GSI) and their applicability to stability of slopes. Int J Rock Mech Min Sci 36:743–760

Walton G, Arzua J, Alejano LR, Diederichs MS (2014) A laboratory-testing-based study on the strength, deformability, and dilatancy of carbonate rocks at low confinement. Rock Mech Rock Eng 48(3):941–958

Walton G, Hedayat A, Kim E, Labrie D (2017) Post-yield strength and dilatancy evolution across the brittle-ductile transition in Indiana limestone. Rock Mech Rock Eng 50(7):1691–1710

Wu S, Zhang S, Zhang G (2018) Three-dimensional strength estimation of intact rocks using a modified Hoek-Brown criterion based on a new deviatoric function. Int J Rock Mech Min Sci 107:181–190

Zandarin MT, Alonso E, Olivella S (2013) A constitutive law for rock joints considering the effects of suction and roughness on strength parameters. Int J Rock Mech Min Sci 60:333–344

Zhang L (2008) A generalized three-dimensional Hoek-Brown strength criterion. Rock Mech Rock Eng 41:893–915

Zhang L (2016) Engineering properties of rocks. Elsevier Ltd, Amsterdam

Zhang L, Zhu H (2007) Three-dimensional Hoek-Brown strength criterion for rocks. J Geotech Geoenviron Eng ASCE 133(9):1128–1135

Zhang Q, Zhu H, Zhang L (2013) Modification of a generalized three-dimensional Hoek-Brown strength criterion. Int J Rock Mech Min Sci 59:80–96

Zhang Y, Feng XT, Yang CX et al (2019) Fracturing evolution analysis of Beishan granite under true triaxial compression based on acoustic emission and strain energy. Int J Rock Mech Min Sci 117:150–161

Zhao XG, Cai M (2010) A mobilized dilation angle model for rocks. Int J Rock Mech Min Sci 47(3):368–384

Zhu H, Zhang Q, Huang B, Zhang L (2017) A constitutive model based on the modified generalized three-dimensional Hoek-Brown strength criterion. Int J Rock Mech Min Sci 98:78–87